JOURNAL OF Applied Polymer SCIENCE

Evaluation of the Processability of Boron-Containing Organosilazane Polymers Based on Shear Rheology

Ting Ouyang,[1,2*] Laura Gottardo,[2†] Samuel Bernard,[3*] Rodica Chiriac,[2] Corneliu Balan,[1*] Philippe Miele[3]

[1]REOROM Laboratory, Hydraulics Department, "Politehnica" University of Bucharest, SplaiulIndependentei 313, 060042 Bucharest, Romania

[2]Laboratoire des Multimatériaux et Interfaces (UMR CNRS 5615), Université Lyon1, 43 Boulevard du 11 Novembre 1918, 69622 Villeurbanne Cedex, France

[3]Institut Européen des Membranes (UMR CNRS 5635), IEM/ENSCM/Université Montpellier 2, Place E. Bataillon, 34095 Montpellier Cedex 5, France

*Present address: College of Material Science and Engineering, Hunan University, 410082 Changsha, China

†Present address: EMPA, Laboratory for Advanced Fibers, Swiss Federal Laboratories for Materials Science and Technology, Lerchenfeldstrasse 5, 90140 St. Gallen, Switzerland

Correspondence to: S. Bernard (E-mail: samuel.bernard@iemm.univ-montp2.fr) or C. Balan (E-mail: corneliu.balan@upb.ro)

ABSTRACT: The shear rheology of boron-containing organosilazane polymers has been investigated in detail with a double objective. The first objective was to evaluate their processability to form fibers by melt-spinning, and the second objective was to predict their molecular structure. We focused on a representative type of boron-containing organosilazane polymers called boron-modified polysilazanes (BmPSs) with the ideal structure $[B(C_2H_4SiCH_3NCH_3)_3]_n$ (C_2H_4 = $CHCH_3$, CH_2CH_2). Characterization tools showed that their viscous and elastic properties are strongly affected by molecular parameters fixed during synthesis and in particular by the methylamine (MA) : tris(dichlorosilylethyl)borane (TDSB) molar ratio imposed during their synthesis. In the spinning domain, the frequency dependences of the storage and loss moduli showed that the prerequisite conditions for obtaining polymer fibers are fulfilled with samples having 9.0 $\leq$ MA : TDSB molar ratios $\leq$ 9.7. However, the presence of thickening in the computed extensional viscosity function and the loss of cohesion of filament derived from samples with MA : TDSB ratio $>$ 9.2 during drawing put in evidence the best potential of polymers with 9 $\leq$ MA : TDSB ratio $\leq$ 9.2 to generate fine-diameter solid filaments in a stable process. Based on rheological tests, the molecular structure of BmPSs has been tentatively predicted in relation with the MA : TDSB ratio. The increase of the latter favored the disentanglement of the polymer framework, and we postulated that it lowered the molecular weight. © 2012 Wiley Periodicals, Inc. J. Appl. Polym. Sci. 000: 000–000, 2012

KEYWORDS: fibers; polysilanes; rheology; processing

Received 22 November 2011; accepted 5 June 2012; published online
DOI: 10.1002/app.38180

INTRODUCTION

Organosilazane polymers are a fascinating class of preceramic polymer that generally displays shaping capability to form "near-net-shape" materials in a large range of compositions.[1–6] They represent inorganic compounds with a skeletal structure that does not only include carbon and silicon atoms but also oxygen and/or nitrogen. The best representative inorganic polymers are poly(carbo)siloxanes and poly(carbo)silazanes that are used in a large domain of applications in their polymeric state and also after shaping and pyrolysis to be converted into ceramics that are called polymer-derived ceramics (PDCs).[1]

The molecular and structural origins of organosilazane polymers such as their degree of crosslinking and/or the nature of the peripherical organic groups, which are linked to the basal polymer network, are key parameters that predetermine their processability in the liquid state or in the molten state if solid and therefore their application. Indeed, it is usually required that the selected preceramic polymer is able to be tractable, thereby to propose a wide range of viscoelastic properties that render it potential for shaping processes such as melt-spinning,[7,8] solution spinning including electrospinning,[9] or liquid phase infiltration of (nano)porous supports.[10,11] This is usually made not

Additional Supporting Information may be found in the online version of this article.

Applied Polymer SCIENCE

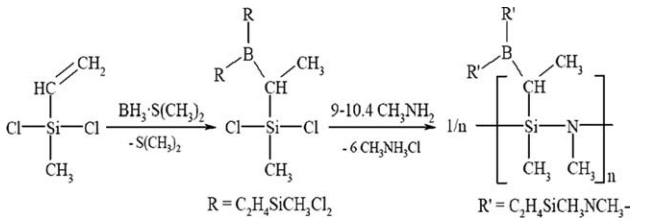

Figure 1. Ideal structure of BmPSs of the type $[B(C_2H_4SiCH_3NCH_3)_3]_n$ (C_2H_4 = $CHCH_3$, CH_2CH_2).

only by designing their chemical composition but also by tailoring the arrangement of their molecular structure. However, controlling the various requirements to process organosilazane polymers and combining them in only one polymer framework is an ambitious objective that is difficult to realize. This is particularly the case for organosilazane polymers devoted to melt-spinning in which processing operations are dominated by stretching deformations.

The melt-spinning behavior of preceramic polymers is far from conventional polymers mainly because of their viscosity, which is considerably more temperature, oxygen, and moisture-sensitive than most of the conventional melt-spinnable polymers or resins. Their viscoelastic properties are very specific,[12–14] and hence the data obtained for conventional polymers melts[15] cannot be directly extrapolated in preceramic and in particular organosilazane polymers. In this particular case, the performing of rheological measurements is extremely difficult. On the other hand, their molecular weight can be reduced in some case by $\sim$ 100 in comparison with the molecular weight measured for conventional polymers melts.

Herein, we focused on a recently discovered category of organosilazane polymers that incorporate boron atoms. They are called boron-modified polysilazanes (BmPSs).[16–23] BmPSs, which ideally displays a molecular structure described as $[B(C_2H_4SiCH_3NR)_3]_n$ (C_2H_4 = $CHCH_3$, CH_2CH_2; R = H,[16–18] CH_3[19–23]), are prepared by reaction of tris(dichloromethylsilylethyl)borane [TDSB, $B(C_2H_4SiCH_3Cl_2)_3$ (C_2H_4 = $CHCH_3$, CH_2CH_2)] with ammonia[16–18] or methylamine (MA, CH_3NH_2)[19–23] followed by the condensation to develop the polymeric network. The current study concerns those prepared with MA leading to BmPSs of the type $[B(C_2H_4SiCH_3NCH_3)_3]_n$ (Figure 1). The control of the MA : TDSB ratio during the polymer synthesis allows us to adjust the degree of crosslinking of the BmPSs and hence to tune their viscoelastic properties in the molten state for melt-spinning.[23] The benefit of rheologists is fundamental in the establishment of relationships between viscoelastic properties and spinning behaviors as well as in the prediction of the molecular structure of these preceramic polymers. This will help chemists to control the synthesis and processability of preceramic polymers that are expected to become a challenging topic for the close future, for example, in energy and microelectronics.

In this article, we provide a detailed picture of the influence of the polymer synthesis parameters on the viscoelastic behavior of BmPSs of the type $[B(C_2H_4SiCH_3NCH_3)_3]_n$. In addition, we predict fundamentally important issues regarding melt-spinning behavior of these polymers, including the computation of elongational spinning viscosity. The obtained rheology is useful not only in adjusting the melt-spinning conditions of this particular class of BmPSs but also in the design of their molecular structure rendering rheology usable as an analytical tool for molecular chemistry. The results described here have the potential to be used for a large variety of preceramic polymers.

EXPERIMENTAL

General Comment

All synthesis reactions were carried out in a purified argon atmosphere passing through successive columns of silica-magnesium oxide support (BTS catalyst) and phosphorus pentoxide by means of standard Schlenk manipulations and vacuum/argon-line techniques. Dichloromethylvinylsilane (CH_2=$CHSiCH_3Cl_2$) was obtained from Sigma-Aldrich (France) and freshly distilled from magnesium at 115°C at P_{atm} before use. Borane dimethylsulfide $BH_3{\cdot}S(CH_3)_2$ (2*M* solution in toluene) was obtained from Sigma-Aldrich and used without further purification. MA anhydrous (>99%; Sigma-Aldrich (France)) was used as received. Tetrahydrofuran (THF) and toluene were purified by distillation from sodium using benzophenone. Manipulation of the chemical products was made inside an argon-filled glove box (Jacomex BS521, Dagneux - France) dried with phosphorus pentoxide.

Polymer Synthesis

BmPSs were obtained by hydroboration of CH_2=$CHSiCH_3Cl_2$, then aminolysis of $B(C_2H_4SiCH_3Cl_2)_3$ (TDSB, C_2H_4 = $CHCH_3$, CH_2CH_2) derived there from and followed standard procedures.[16–26] The intermediate yellow oil TDSB was purified by vacuum distillation (3×10^{-2} mbar/117°C) via an ether bridge to deliver a colorless oil before aminolysis with MA. NMR and elemental analysis results fitted those reported in the literature.[24–26] The synthesis of BmPSs of the type $[B(C_2H_4SiCH_3NCH_3)_3]_n$ (C_2H_4 = $CHCH_3$, CH_2CH_2) was performed from TDSB in THF at 0°C. MA was trapped in a Schlenk tube in liquid air, and accordingly, a corresponding amount of TDSB was precisely adjusted into the Schlenk flask. The Schlenk tube containing MA was connected to the cooled Schlenk flask containing THF solution of TDSB and removed from the liquid air cooling bath. Both parts were linked via an interconnection flexible tube, which was evacuated and then refilled with argon. Argon was slowly introduced in the Schlenk tube containing MA, and after the central valve was opened, MA was allowed to warm up to room temperature (RT) to be passed through the solution at 0°C under vigorous stirring. When addition was complete, the mixture was allowed to warm to 25°C and kept at this temperature under vigorous stirring overnight. The solution was then separated from the precipitate by filtration through a pad of Celite. The solvent was removed by distillation (RT/1.5×10^{-1} mbar) to release air- and moisture-sensitive colorless polymers. The reaction between TDSB and MA proceeded quantitatively; the separation from the byproduct methylamine hydrochloride by filtration resulted in product loss $\leq$ 10%. Using this general procedure, we synthesized a set of representative BmPS (**BmPS9.0** $\rightarrow$ **BmPS10.4**) by deliberately changing the MA : TDSB ratio. Table I reports some properties for each of the polymers that have been prepared.

Table I. Properties of BmPSs of the Type $[B(C_2H_4SiCH_3NCH_3)_3]_n$ (C_2H_4 = $CHCH_3$, CH_2CH_2) (**BmPS9** → **BmPS10.4**)

Sample	MA : TDSB ratio	Chemical composition	T_{SDC}[a] (°C)	T_{MDC}[a] (°C)	T^*[b] (°C)	$T_{Spinning}$ (°C)
BmPS9	9	$[Si_{3.0}B_{1.1}C_{11.3}N_{3.3}H_{36.8}]_n$	74	~ 125	106	105-125
BmPS9.2	9.2	$[Si_{3.0}B_{1.1}C_{11.8}N_{3.6}H_{37.7}]_n$	70	~ 125	85	98-120
BmPS9.7	9.7	$[Si_{3.0}B_{1.1}C_{12.2}N_{3.8}H_{39.6}]_n$	60	~ 125	77	95-115
BmPS10.4	10.4	$[Si_{3.0}B_{1.1}C_{12.5}N_{4.3}H_{41.2}]_n$	52	~ 95	71	Capillary instability

[a]Value measured for a pressure of 0.025 MPa corresponding to the TMA displacement of 95% in Figure 3(a), [b]Value corresponding to the maximum dTMA rate in Figure 3(b).

It is important mentioning that a MA : TDSB ratio higher than 10.6 involved a change in the physical state of the polymer leading to a viscous BmPS whose viscoelasticity is not tailored for melt-spinning. Therefore, only 9 ≤ MA : TDSB ratio < 10.6 is considered in this study; however, such a result will be taken into account for discussion.

Melt-Spinning

Preceramic fibers were prepared by polymer melt-spinning in a nitrogen atmosphere using a lab-scale piston extrusion system (Matériau Ingéniérie-St-Christol les Alès, France). It enables definite throughputs and specific adjustment of fiber dimensions by properly adjusting the take-up velocity of the wind-up spool. Polymers **BmPS9** → **BmPS10.4** (2.5 g) were molten by heating within a heater block until an appropriate viscosity was obtained and progressively compacted by a piston. The molten polymer flowing was then driven through heated elements containing filter and spinneret having a single capillary according to Figure 2. The experimental setup and the visualization system are available in Supporting Information Figure S1.

In the present configuration, $D = 9.55$ mm is the piston diameter, $d_0 = 0.2$ mm is the capillary diameter, and $h = 1$ mm its length. $d_i \cong 1.2\ d_0$ is the maximum-swell fiber diameter (located at distance $\delta \cong 0.6\ d_0$ from the exit) and $d_f \cong 8\ \mu$m is the spun diameter. The resulting polymer emerging from the capillary at an ideal load of ~ 350 N as an endless filament was stretched and continuously collected on a rotating spool. The distance from the rotating spool to the spinneret was fixed at 13 cm. Extrusion and drawing units are designed for small-scale spinning and can support stable flow rates from 10 to 400 $mm^3\ min^{-1}$ throughputs from 0.1 to 2 mm min^{-1} and take-up velocity from 9 to 330 m min^{-1}. Difference responses to melt-spinning were obtained according to the MA : TDSB ratio.

Characterization

Melt-behavior was investigated by thermomechanical analysis (TMA, Mettler Toledo TMA/SDTA 840) on polymer pellets in a nitrogen atmosphere from 30 to 150°C at a heating rate of 5°C min^{-1} using a pressure of 0.025 MPa. Thermal properties have also been studied by differential scanning calorimetry (DSC, Mettler Toledo DSC TA 8000) in an argon atmosphere between −20°C and 125°C at a heating rate of 10°C min^{-1} in aluminum crucibles. Rheological properties of BmPSs have been measured using a Physica MCR 301 rheometer equipped with the Peltier heat and temperature controlled cell up to 180°C. Oscillatory strain and stress controlled experiments have been performed with the plate and plate geometry of 25 mm diameter and nominal gap of 0.3 mm. For each sample, several isothermal frequency sweep tests were conducted in the linear viscoelastic regime at the temperature of spinning experiments to establish the reproducibility of the measurements and to investigate the samples stability. Because of the air- and moisture-sensitive properties of BmPSs, the rheological tests are conducted under argon atmosphere, which required a special designed glove box to isolate the measuring geometry from the contact with air (the oxygen content in the glove box was maintained below 1% and moisture at maximum 3% rel.) (See the Physica MCR301 Rheometer with special designed glove-box in Supporting Information Figure S2.) As the polymers are reactive toward moisture and oxygen, the sample preparation was performed within a glove box in an argon environment.

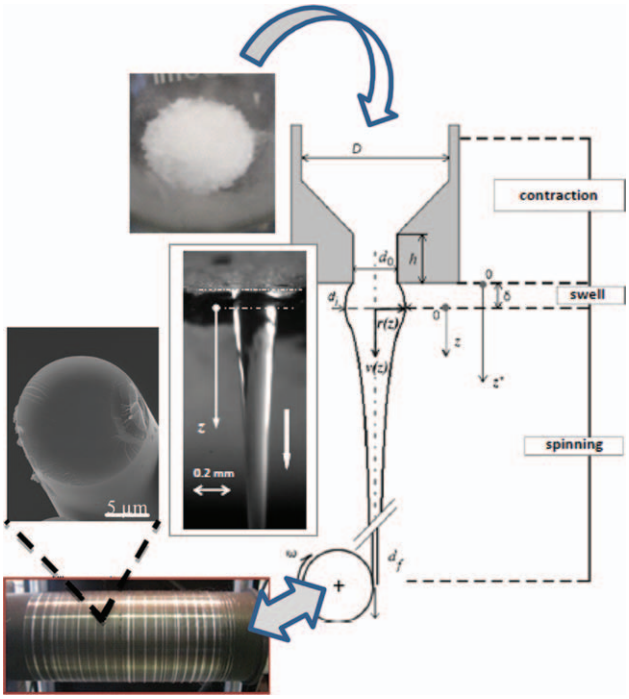

Figure 2. Schematic representation of the fiber-spinning process. The microscopic picture of a typical melt-spinnable BmPS (**BmPS9**) of the type $[B(C_2H_4SiCH_3NCH_3)_3]_n$ (C_2H_4 = $CHCH_3$, CH_2CH_2) during spinning is taken at a extrusion velocity in the die of $v_{Extrusion} \cong 1$ mm min^{-1}; $v_0 \cong 2.2$ m min^{-1}, and at a take-up spool velocity of $v_S \cong 70$ m min^{-1}. [Color figure can be viewed in the online issue, which is available at wileyonlinelibrary.com.]

RESULTS AND DISCUSSION

In this work, we firstly synthesized BmPSs making use of the Schlenk-type synthesis procedure combined with vacuum-argon lines. Secondly, we investigated TMA to evaluate the plastic deformation of BmPSs and we tested them with regard to melt-spinning. Thirdly, their shear rheology has been investigated in the spinning domain. Based on these results, we are able to provide the appropriate synthesis conditions to deliver BmPSs with tuned viscoelastic properties and tailored melt-spinnability. In addition, we are able to predict their molecular structure according to the MA : TDSB ratio based on TMA and shear rheology results.

Polymer Synthesis

The basal structure of BmPSs of the type $[B(C_2H_4SiCH_3NCH_3)_3]_n$ is expected to be composed of polysilazanes rings $[—Si—N—]_n$[16] crosslinked via $B(C_2H_4)_3$ bridges with $C_2H_4 = CHCH_3$ and CH_2CH_2 (Figure 1). In our case, CH_3 groups are linked to both Si and N atoms.

It is generally admitted that synthesis parameters affect the plastic deformation and the viscoelastic behavior of polymers. Here, this was confirmed by changing the MA : TDSB ratio fixed during BmPSs synthesis. Indeed, we observed that MA : TDSB ratios higher than 9 allow us to deliver solid BmPSs, which propose different responses to melt-spinnability. Furthermore, MA : TDSB ratios higher than 10.6 lead to viscous polymers that were unable to provide melt-spinning properties. Within this context and according to the fact that melt-spinnability is directly affected by rheology, we synthesized a set of representative BmPSs with $9 \leq$ MA : TDSB ratio < 10.6 to scan a large domain of rheological behaviors. Four BmPSs with controlled MA : TDSB ratios (**BmPS9** → **BmPS10.4**) have thus been synthesized according to the experimental protocol described in the experimental part to be characterized by TMA and shear rheology.

Thermomechanical Behavior of BmPSs

TMA has been investigated under nitrogen using a pressure of 0.025 MPa up to 170°C. Figure 3 presents the TMA curves of samples **BmPS9** → **BmPS10.4** [Figure 3(a)] and the corresponding rates of displacement [Figure 3(b)] as a function of the temperature.

In such experiments, we have monitored the dimensional changes of samples that occurred during their heat treatment at low temperatures under a compressive load.[27] TMA experiments give us the temperature range at which samples start to soften.

Figure 3(a) shows that an increase of the MA : TDSB ratio from 9 to 10.4 shifts the temperature of the starting of the dimensional change (T_{SDC}) to lower temperatures, without changing both the magnitude of the final plastic deformation and the TMA curve profile. In particular, polymers are seen to strongly shrink in thickness as illustrated by the maximum dimensional change which is measured ($\sim$ 95%). In contrast to T_{SDC}, the temperatures at which the dimensional change is maximum (T_{MDC}) occurs at the same temperature ($\sim$ 125°C) for **BmPS9** → **BmPS9.7**. It occurs at $\sim$ 95°C for **BmPS10.4** before swelling ($\sim$ 107°C) and re-softening ($T > \sim$ 107°C). The almost complete dimensional changes of BmPSs indicates a very high capability to soften on heating. The associated dTMA curves [Figure 3(b)] highlights a simple deformation behavior for the sample **BmPS9**, whereas dTMA behaviors become more and more complex for samples **BmPS9.2** to **BmPS10.4**. The corresponding curves are made of several deformation peaks with a maximum corresponding to T^*. Table I reports the values of T_{SDC}, T_{MDC}, and T^*. The increase of the complexity of the plastic deformation with the increase of the MA : TDSB ratio clearly indicates a decrease of the molecular weight distribution of the polymer. In association with the decrease of the values of T_{SDC} with the increase of the MA : TDSB ratio, we tentatively postulated that a decrease of the molecular weight continuously occurred from **BmPS9** to **BmPS10.4**. This can be explained as follows. Because of the high mobility of molecules in the softened state, response due to this mobility will play a major role along with the effect of entanglement loosening, which will make the behavior become more complex for samples **BmPS9.7** → **BmPS10.4**. In contrast, the complexity of

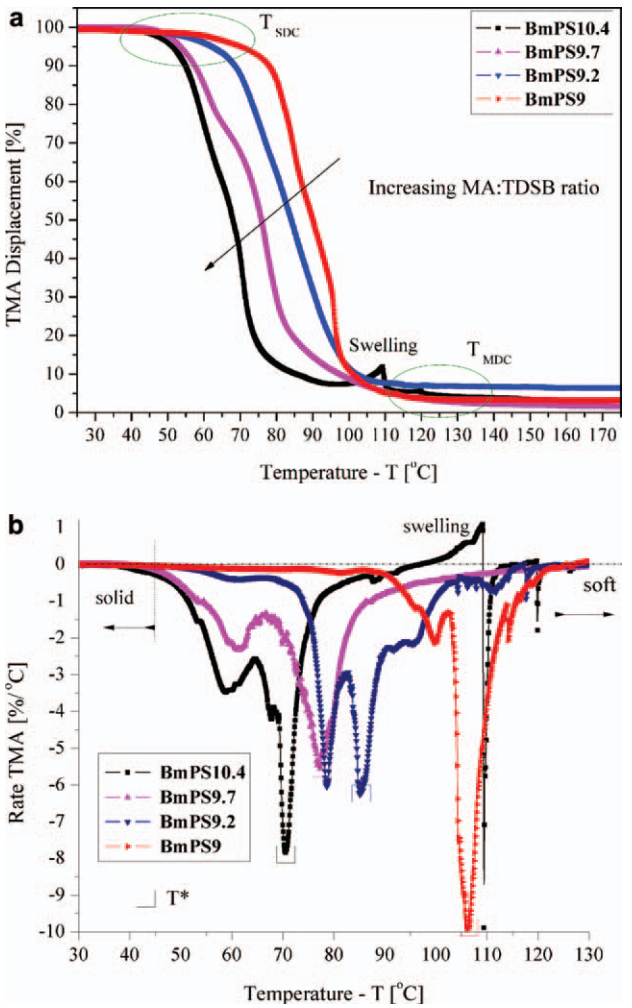

Figure 3. TMA graphs of samples **BmPS9** → **BmPS10.4**: displacement (dimensional change) versus temperature (a) and rate of displacement versus temperature (b). [Color figure can be viewed in the online issue, which is available at wileyonlinelibrary.com.]

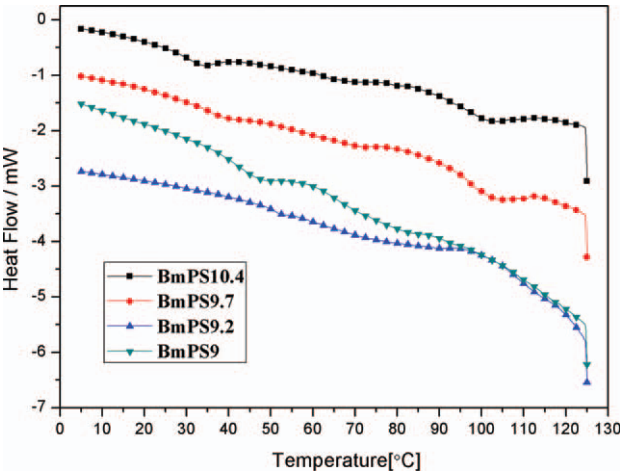

Figure 4. DSC graphs of samples **BmPS9 → BmPS10.4**. [Color figure can be viewed in the online issue, which is available at wileyonlinelibrary.com.]

BmPS9 is the least one because of the higher molecular weight achieved in this sample. The effect of molecule entanglements will prevail for higher temperature and in certain temperature will start to loosen.

TMA experiments predicted that BmPSs exhibits potentialities to be extruded in the temperature range T_{SDC}–T_{MDC}. Table I reports the values of the spinning temperature ($T_{Spinning}$) measured for each of the samples during melt-spinning experiments. As indicated in Table I, spinning of BmPSs occurs in a relatively large range of temperature and it almost corresponds to the maximum dimensional change reached by the polymer. Moreover, the evolution $T_{Spinning}$ as a function of the MA : TDSB ratio follows the evolution of T_{SDC} and T^*, that is, $T_{Spinning}$ decreased with the increase of the MA : TDSB ratio. As a particular case, the sample **BmPS10.4** did not exhibit proper spinnability because it was too fluid to be properly extruded without capillary instability. This can be linked to a poor chain entanglement and/or a low molecular weight.

An important requirement for melt-spinning is that polymers must be thermally stable during melt-spinning to provide reliable rheological data. TMA and corresponding dTMA curves showed that only the sample **BmPS10.4** (the highest MA : TDSB ratio) exhibits a local swelling during melting most probably due to polymer decomposition at this temperature. This is highly reflected by DSC measurements. It should be mentioned that the glass transition of samples **BmPS9 → BmPS10.4** measured by DSC extends over a wide temperature range (∼ 20°C), which may be interpreted as a high molar mass dispersion in polymers. They transform into viscous materials by passing through T_g values taken at the middle of the temperature range, which decreases with the increase of the MA : TDSB ratio from 51 to 32°C (Figure 4). Above the glass transition, the samples **BmPS9 → BmPS9.2** seem to remain stable up to 125°C, whereas a small exothermic peak due to the polymer decomposition is observed for samples **BmPS9.7** and **BmPS10.4** around 105 and 100°C, respectively. This is particularly obvious for the sample **BmPS10.4**, which can explain its swelling observed by TMA.

Rheological Properties

Based on TMA results and melt-spinning tests that demonstrated the relatively large temperature of spinning, we decided to perform rheological tests at 115°C. This temperature is in the melt-spinning domain of samples **BmPS9 → BmPS9.7**. Here, we investigated the shear dynamics rheology of samples **BmPS9 → BmPS9.7** by plotting the frequency dependence of the dynamics moduli G' (elastic/storage modulus) and G'' (viscous/loss modulus) as well as the damping factor tan δ at 115°C. We also investigated the evolution of the complex viscosity η^* as a function of the oscillatory frequency. It has to be mentioned that the sample **BmPS10.4** could not be considered here because it exhibits a negligible elasticity.

As-plotted curves help us to correlate the viscoelastic properties of samples **BmPS9 → BmPS9.7** with the melt-spinnability:

- The G''-to-G' ratio, that is, tan δ, is closely correlated to polymer spinnability,[12–14] as this process requires an appropriate viscosity-to-elasticity ratio (tan $\delta > 1$) allowing deformation of the polymer melts by flowing through the spinneret and then retention of the filament shape at the capillary exit.
- The elastic modulus is linked to the drawing ability of the emerging molten filament, which must exhibit a minimum level of elasticity to ensure cohesion of the fiber along the spinning line and then retention of the fiber shape as it solidifies.[12,28]

Assuming the Cox-Merz relation[29] to be applied, we considered that the oscillatory frequency ω is related to the shear rate within the capillary and with the extensional strain rate within and downstream the capillary.[30] Therefore, the results from oscillatory shear tests can be used to analyze the spinning quality of the polymer melt.

Figure 5 shows the variation of dynamics moduli, complex viscosity η^*, and tan δ as a function of the oscillatory frequency for samples **BmPS9 → BmPS9.7** at 115°C.

The tests from Figure 5 consist in the frequency sweep tests at constant strain amplitude ($\gamma_a = 0.01$ [−]), within the linear viscoelastic range. Even if the experiments have been performed in a controlled closed atmosphere, the small amount of remaining moisture and oxygen from inside the box influenced the chemical stability of samples at larger experimental times than 10 min. Therefore, the tested frequency domain has been limited at $\omega = 1$ rad s^{-1}. We mention that experiments from Figure 5 were repeated three times each with new samples, with the results being reproducible.

Regarding storage and loss moduli as a function of frequency [Figure 5(a)], it can be seen that samples **BmPS9 → BmPS9.7** exhibit a close behavior: they reveal an increase of the magnitude of G'' with increasing oscillatory frequency, which is due to the higher energy required for molecular viscous response. The frequency domain corresponds to the plateau and transition regions, which indicate the dominance of relatively long (for a preceramic network) fragments of polymer chains and the effect of chain branching.[14] The slight increase of the magnitude of G' within the plateau region for melted **BmPS9 → BmPS9.7** is attributed to a decrease in time available for

Applied Polymer SCIENCE

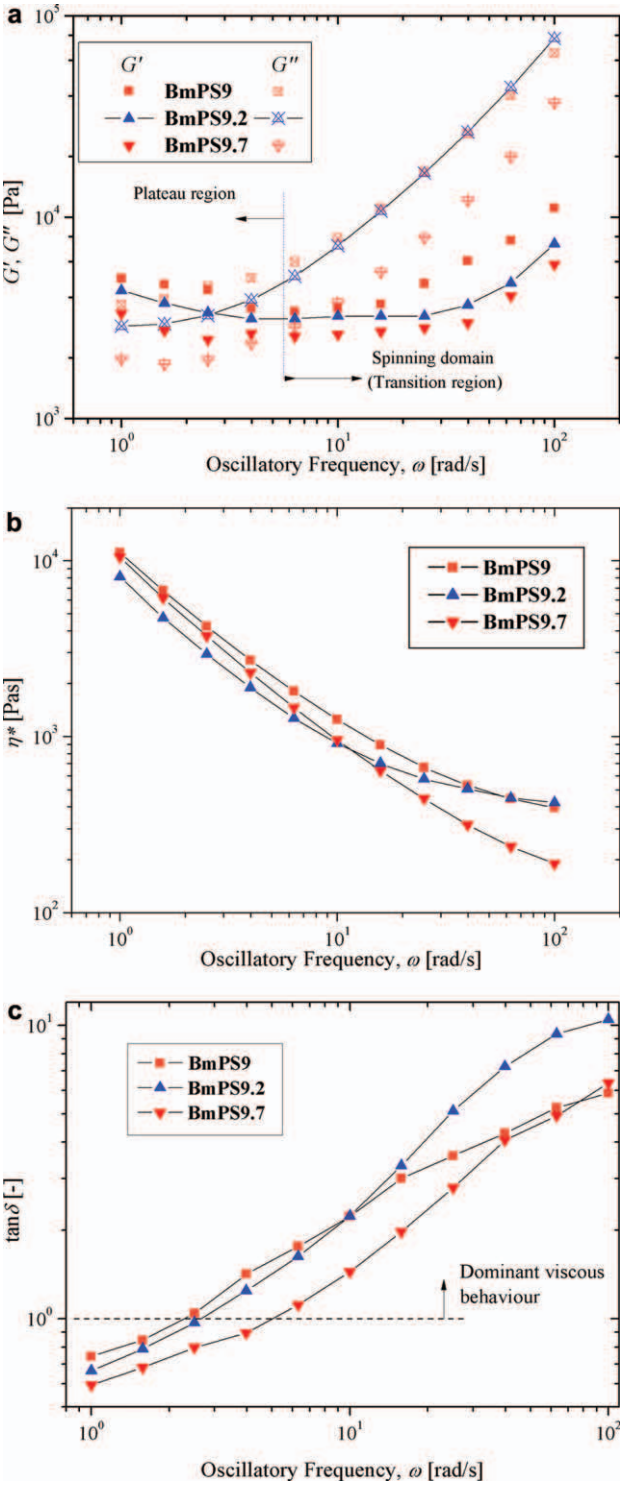

Figure 5. Rheological characterization of samples **BmPS9.2** → **BmPS9.7** at 115°C: dependence with frequency of dynamics moduli (a), complex viscosity (b), and damping factor (c). [Color figure can be viewed in the online issue, which is available at wileyonlinelibrary.com.]

molecular relaxation. The elasticity is dominant for all samples (i.e., $G' > G''$) in the low regime of the frequency range: $\omega < 3$ rad s^{-1} for **BmPS9** and **BmPS9.2** and $\omega < 5$ rad s^{-1} for **BmPS9.7** [see Figure 5(c)]. At a certain frequency, the crossover of G' and G'' occurs and the viscous component becomes larger than the elastic component, which signifies the onset of transition between plateau and glassy regions.

The oscillatory frequency position of this crossover point increases from 1.6 rad s^{-1} for **BmPS9** and **BmPS9.2** to 4.5 rad s^{-1} for **BmPS9.7**. This means that it is required to apply a higher oscillatory frequency, thus a higher extrusion velocity, to extrude **BmPS9.7** in comparison with **BmPS9** and **BmPS9.2** at the same spinning pressure. This was confirmed by melt-spinning tests. However, the higher extrusion velocity to be applied to **BmPS9.7** requires a higher take-up velocity to reach the same filament diameter during melt-spinning process of **BmPS9.7** in comparison with **BmPS9** and **BmPS9.2**. This inherently caused the loss of cohesion of the **BmPS9.7**-derived filament, as its elasticity is lower in comparison with the other samples.

As shown in the log–log plots in Figure 5(b), the complex viscosity η^* of **BmPS9** → **BmPS9.7** follows the same trend. It is seen to continuously decrease in the oscillatory frequency range 0.25–100 rad s^{-1}. This indicates the shear-thinning behavior of BmPSs. This non-Newtonian behavior is becoming more pronounced with increasing MA : TDSB ratio. The lower magnitude of η^* for **BmPS9.7** in comparison with the values measured for **BmPS9** → **BmPS9.2** at a given ω (especially at high oscillatory rate) indicates an increase of the chain mobility in the corresponding sample; thereby a probable decrease of the relative amount of crosslinked portions going from **BmPS9** to **BmPS9.7**. In addition, the samples **BmPS9** and **BmPS9.2** disclose a reduced shear-thinning at high rates, which is expected to stabilize the flow of the emerging fiber during drawing at high tale-up velocity which is not the case for **BmPS9.7**. This was confirmed with melt-spinning tests that showed a loss of cohesion of the **BmPS9.7**-derived filament under drawing at high take-up velocity.

The current observation confirms that rheological behavior and melt-spinnability are rather governed by the crosslinking density of the polymer network. The melt-spinnability criteria were introduced in our previous studies[12,14] based on the parametric plot: G' versus tan δ (Figure 6). An excess of the viscous component over the elastic one, that is, tan $\delta > 1$ is required for melt extrusion and a minimum elasticity component is needed to keep the fiber continuity during spinning. Based on such requirements, Figure 6 shows that proper spinning of **BmPS9** → **BmPS9.7** can be located above $G' = 3 \times 10^3$ Pa.

Furthermore, based on the decreased melt-spinnability from **BmPS9** to **BmPS9.7**, that is, the increase of the loss of cohesion of the filament on drawing, it is reasonable to fix a maximum for tan δ at 5. As a consequence, a maximum value of elasticity can be fixed at 5×10^3 Pa.

For a given molecular weight, the correlation of elasticity with the damping factor is determined by the polymer crosslinking and chain mobility. The limits of spinning domain from Figure 6 are experimentally established for each sample and working conditions; however, general requirements of melt rheology were observed for a proper fiber-spinning process,[13,14,28] that is, $1 < \tan \delta < 5$, 10^3 Pa $< G' < 10^5$ Pa.

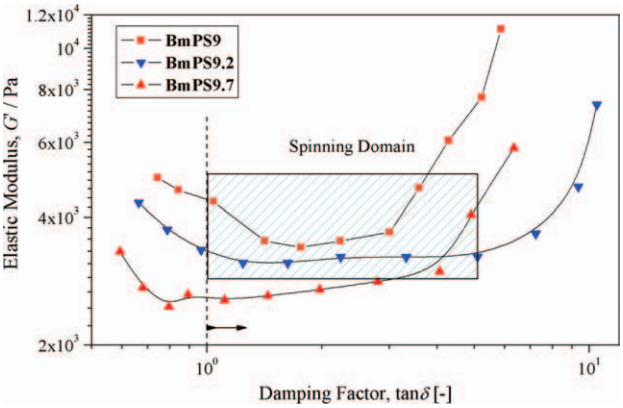

Figure 6. Change of G' versus tan δ for samples **BmPS9** → **BmPS9.7**; the proper spinning domain is marked. [Color figure can be viewed in the online issue, which is available at wileyonlinelibrary.com.]

A complete rheological characterization of a complex fluid requires investigations both in shear and elongational motions. Downstream the die (see Figure 2), the fiber spinning of polymer melts is a pure extensional flow.[31] As consequence, the extensional viscosity is the main material function that characterizes the polymer rheology during spinning,

$$\eta_e = \frac{\sigma_{zz} - \sigma_{rr}}{\underline{\varepsilon}}, \tag{1}$$

where $\sigma_{zz} - \sigma_{rr}$ is the extensional tensile stress and $\underline{\varepsilon} = \frac{dv_z}{dz}$ is the corresponding strain rate.[15,31]

To measure the extensional (spinning) viscosity of air sensitive polymer melts, in particular the BmPS samples, involves developing of a complex setup within the close test chamber, which allows the visualization of the fiber, that is, the measurement of the radius profile, $r = R(z)$ along z-spinning direction (see Figure 2 and Supporting Information Figure S1). In a stationary flow, within a thin symmetric fiber, one can assume that velocity v_z is constant at constant z-coordinate, the flow rate and tensile force being maintained constant along the fiber:

$$R^2 v_z = C_1 \text{ and } R^2(\sigma_{zz} - \sigma_{rr}) = C_2, \tag{2}$$

where C_1 and C_2 are appropriate constants.

Therefore, the extensional viscosity has the nondimensional form as follows:

$$\eta_e = \frac{f(0)}{f(\bar{z})}, \tag{3}$$

where $f(\bar{z}) = \frac{2}{\bar{R}}\frac{d\bar{R}}{d\bar{z}}$, with boundary condition $\eta_e = 1$ at $\bar{z} = 0$ (the reference space scale being the radius of the die, R_0). In eq. (3), the extensional viscosity is dependent on both strain rate and temperature.

For the process under investigation, the energy conservation[31,32] takes the nondimensional expression:

$$Pe\frac{dT}{d\bar{z}} + 2Bi(T - T_a) = Br\eta_e g(\bar{z}). \tag{4}$$

Here, $g(\bar{z}) = \frac{4}{\bar{R}^4}\left(\frac{d\bar{R}}{d\bar{z}}\right)^2$, T_a is the ambient temperature and T is the current temperature of the fiber (normalized with T_0 the temperature at the exit of the die); $Pe = \frac{\rho c_p R_0 v_0}{k}$, $Bi = \frac{\alpha R_0}{k}$, $Br = \frac{\eta_0 v_0^2}{T_0 k}$ are the Péclet, Biot, and Brinkman numbers, respectively (ρ and η_0 are the density and zero shear viscosity of the sample; C_p, α, and k are the specific heat, surface heat transfer coefficient, and the thermal conductivity; and v_0 being the average velocity at the extrusion from the die).

Influence of temperature variation along the fiber (including solidification and crystallization phenomena) on the melt-spinning simulations are investigated in several studies[29,32–35]; however, direct measurements of temperature variation along a thin fiber are not yet published.

The algorithm for computing the nondimensional extensional viscosity[36] is based on the direct measurement of the radius profile $R(z)$. For a known function $\bar{R}(\bar{z})$, the extensional viscosity can be obtained from by eq. (3), and the temperature profile $\bar{T}(\bar{z})$ is computed from (4) for characteristic values of nondimensional numbers. Assuming a temperature dependence of extensional viscosity of the form:

$$\eta_e = \eta_{e0}(\underline{\varepsilon})\exp\left[\kappa\left(\frac{1}{T} - 1\right)\right], \tag{5}$$

where $\kappa = \frac{E}{RT_0}$ (E is the activation energy and R is the gas constant), and finally the extensional function at constant temperature, $\eta_{e0}(\underline{\varepsilon})$, is obtained.

Pictures of the fibers were analyzed for a length of $5d_0$ starting from the exit from spinneret using the setup from Figure 2 and specialized image analysis software. In analysis of the acquired picture, under the same visualization conditions, pictures of a diameter-known fiber of PCS sample (polycarbosilane classical melt-spinnable preceramic polymer from Sigma Aldrich) are first taken as a reference.[36] Calibration is done according to the reference, and measurement of diameter along the spinline is obtained by using Image-Pro Plus. The error tolerance is around 1% for the measurements.

We have recorded and fitted the diameter profile of as-extruded fibers derived from **BmPS9** and **BmPS9.2** during drawing (Figure 7).

The drawing fibers of **BmPS9.7** were not stable: they are not axial symmetric and disclose oscillations for the tested take-up velocities. The properties and boundary conditions used for computation of extensional viscosity of **BmPS9** sample are listed in Table II.

Accordingly to the described computational procedure, the set of simulation results are reported in Figure 8 for the sample **BmPS9** (we expect a qualitative similar behavior for **BmPS9.2** melt).

The nondimensional viscosity functions presented in Figure 8 is obtained numerically by computation of the steady, incompressible one-dimensional fiber flow, taking into account the heat transfer. The temperature variation along the spinning line ($0 < z < 5{\cdot}d_0$) is monotonous due to cooling and the corresponding increase of extensional viscosity with the temperature decrease

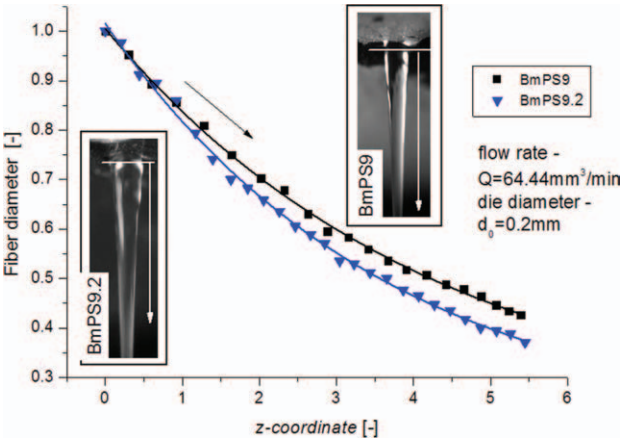

Figure 7. Variation of nondimensional fiber diameter along the spin line for samples **BmPS9** ($v_f \cong 70$ m min^{-1}) and **BmPS9.2** ($v_f \cong 110$ m min^{-1}), respectively. [Color figure can be viewed in the online issue, which is available at wileyonlinelibrary.com.]

[see Figure 8(a)]. The dependence of extensional viscosity function against the local strain rate at constant temperature [Figure 8(b)] discloses the presence of strain-hardening phenomena (decreasing followed by increasing of extensional viscosity with increasing of strain rate). This behavior indicates an extension thickening for BmPSs of the type $[B(C_2H_4SiCH_3NCH_3)_3]_n$, which is normally associated with long-chain branches, nonlinearity, and high molecular mass of the polymer.[37]

The spinning experiments and computed extensional viscosity are both consistent with the rheological characterization of the samples in oscillatory shear flows. The synthetic results from Figure 6 indicate that sample **BmPS9.7** is not proper for spinning under normal conditions, which was directly observed in experiments. The good quality of fibers for **BmPS9** and **BmPS9.2** is associated with the strain hardening of the polymers in extension and with a well-defined range for the elastic shear modulus within the fluid domain of the melt (tan $\delta > 1$).

Molecular Structure Prediction

It is clear that the increasing MA : TDSB ratio involves the general decrease of both viscosity and elasticity, the influence being more evident in reducing the complexity of the plastic deformation [Figure 3(b)], the storage modulus [Figure 5(a)], and the complex viscosity [Figure 5(b)]. On the basis of these statements, we can tentatively suggest molecular structures for the series of BmPSs considered here in relation with their MA : TDSB ratio.

There are two configurations that are responsible for the loss of both the complex viscosity and the elasticity. In a first configuration, the polymer is composed of linear parts. In this type of configuration, the lack of strong interaction between the chains provides relatively high molecular motion and therefore adds to the mobility of the polymer backbone. This leads to a predominant viscous character as observed in samples with MA : TDSB ratio higher than 10.6, which are viscous at RT. However, it has been shown that the plastic deformation is shifted to lower temperatures with the increase of the MA : TDSB ratio, indicating decrease in the dispersion of the molecular weight; therefore, probably in the value of the molecular weight. As a second configuration, we therefore suggested the formation of both low-molecular-weight and linear structures with the increase of the MA : TDSB ratio. This configuration involves a decrease in the proportion of constraints for molecular motions to render the corresponding polymer more processable and easier to work on heating, which is the case for samples **BmPS9.7** and **BmPS10.4**.

On the basis of the shear rheology measurements, we can propose two categories of BmPSs: the samples **BmPS9–BmPS9.2** in one hand and the **BmPS9.7–BmPS10.4** in the other hand.

Samples **BmPS9** and **BmPS9.2** probably exhibit characteristics of polysilazanes constituted of $[—Si—N—]_n$ rings with $n = 2,3$ linked by an adequate portion of $B(C_2H_4)_3$ ($C_2H_4 = CHCH_3$, CH_2CH_2) crosslinks as it was proposed by Riedel et al.[16] Their chemical composition tends to demonstrate that their structure is close to that proposed in Figure 1 even if terminating $N(H)CH_3$ groups can explain the deviation of the determined nitrogen, carbon, and hydrogen values from those calculated $[Si_{3.0}B_{1.0}C_{12.0}N_{3.0}H_{30.0}]_n$. This structural configuration decreases the molecular motion to a certain extent, which naturally stiffens the polymer network. However, methyl-linked to Si and N provide sufficient viscosity to overcome elasticity during extrusion that allowed us to appropriately spin samples **BmPS9–BmPS9.2**. Furthermore, the nature of the bridging $B(C_2H_4)_3$ ($C_2H_4 = CHCH_3$, CH_2CH_2) units provides appropriate mobility to the polymer backbone, which is particularly compatible with a drawing at relatively high take-up velocity. In contrast, we speculate that samples **BmPS9.7** and **BmPS10.4** display a structure far from that one depicted in Figure 1. The ideal chemical formulas of both **BmPS9.7** and **BmPS10.4** are $[Si_{3.0}B_{1.0}C_{12.0}N_{3.0}H_{30.0}]_n$, whereas the measured formulas are $[Si_{3.0}B_{1.1}C_{12.2}N_{3.8}H_{39.6}]_n$ and $[Si_{3.0}B_{1.1}C_{12.5}N_{4.3}H_{41.2}]_n$, respectively. Such compositions can be traced back to incomplete transamination of $B[C_2H_4Si(CH_3)(NHCH_3)_2]_3$ ($Si_{3.0}B_{1.0}C_{15.0}N_6H_{45.0}$) during the addition of MA to TDSB that tends to lead to short and poorly entanglemented chains. Such a molecular structure is relatively free to move in cooperative thermal motion to provide conformational rearrangement of the backbone, thus high capability to flow through a spinneret. In contrast, such structural features are an obstacle for the subsequent drawing. All these conclusions are supported by fiber-spinning experiments and the strain hardening of extensional viscosity observed for **BmPS9–BmPS9.2** samples.

The stronger elasticity (recorded both in shear and extension) of **BmPS9–BmPS9.2** samples in comparison with **BmPS9.7–**

Table II. Properties and Boundary Conditions for BmPS9 Sample

η_0 (Pa s)	ρ (kg m^{-3})	k (w m^{-1} K^{-1})	C_p (J kg^{-1} K^{-1})	E (J mol^{-1})	v_0 (m s^{-1})	v_f (m s^{-1})	R_0 (m)	T_0(K)
12,000	1190	0.2–0.5	1140	180×10^3	0.038	1.0	0.0001	388

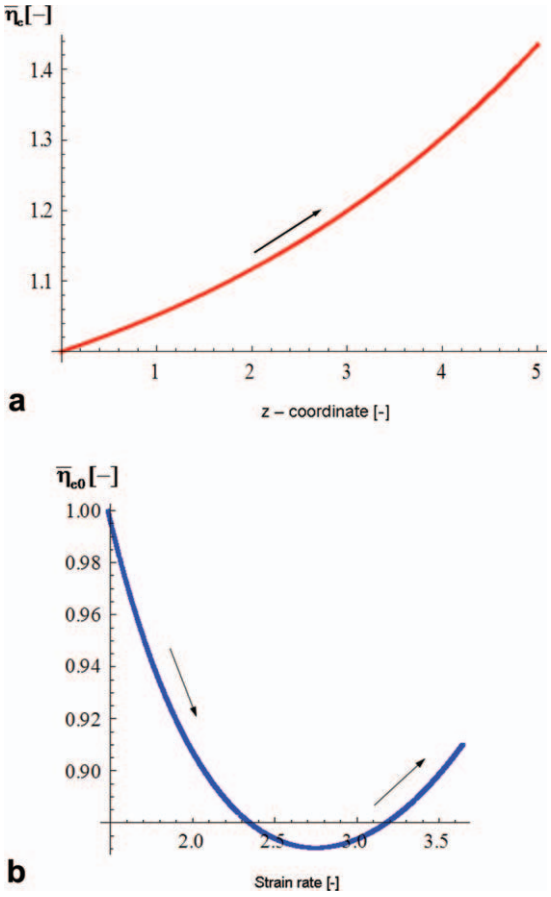

Figure 8. Nondimensional computed extensional viscosities for **BmPS9** sample: (a) variation of extensional viscosity along the fiber (nonisothermal) and (b) extensional viscosity function at constant temperature, see relation (5) and Table II. [Color figure can be viewed in the online issue, which is available at wileyonlinelibrary.com.]

BmPS10.4 indicates a greater potential for boron-modified polysilazanes of the type $[B(C_2H_4SiCH_3NCH_3)_3]_n$ (C_2H_4 = $CHCH_3$, CH_2CH_2) with 9 ≤ MA : TDSB ratio ≤ 9.2 to be drawn into fibers with fine diameters.

CONCLUSIONS

Shear rheology of organosilazane polymers represented by a series of boron-modified polysilazanes of the type $[B(C_2H_4SiCH_3NCH_3)_3]_n$ (C_2H_4 = $CHCH_3$, CH_2CH_2) has been investigated in the molten state by means of TMA and oscillatory shear flow. The aim of this work was to study the role of the shear rheology in the melt-spinning of these polymers and to provide some criteria that predict their melt-spinnability. Experiments showed that plasticity and viscosity of these polymers are strongly affected by the synthesis parameters and especially the MA : TDSB ratio imposed during the polymer synthesis. This is inherently due to a modification of the polymer structure during synthesis. We postulated that an increase of the MA : TDSB ratio led to the general formation of low-molecular-weight compounds. This decreased both plasticity and viscosity; thereby reducing the melt-spinnability. In this study, the most suitable conditions for melt-spinning were investigated from the view point of the complex viscosity, storage modulus, and loss modulus. The complex viscosity η^* is seen to decrease with increasing oscillatory frequency ω, indicating clearly the shear-thinning behavior of polymers with 9 ≤ MA : TDSB ratio ≤ 9.7 during extrusion. The frequency dependences of the storage and loss moduli showed that the prerequisite conditions for obtaining fibers, that is, $1 < \tan\delta < 5$ and 3×10^3 Pa $< G' < 5 \times 10^3$ Pa, are fulfilled for samples with 9 ≤ MA : TDSB ratio ≤ 9.7. However, the presence of thickening in the computed extensional viscosity function put in evidence the best potential of boron-modified polysilazanes of the type $[B(C_2H_4SiCH_3NCH_3)_3]_n$($C_2H_4$ = $CHCH_3$, CH_2CH_2) with 9 ≤ MA : TDSB ratio ≤ 9.2 for drawing the emerging molten filament, as it solidified into a fine-diameter solid filament without loss of cohesion.

ACKNOWLEDGMENTS

The authors thank the European Community for supporting this work through the Marie Curie Research Training Network PolyCerNet (Contract MRTN-CT-2005-019601).

REFERENCES

1. Colombo, P.; Mera, G.; Riedel, R.; Soraru, G. D. *J. Am. Ceram. Soc.* **2010,** *93*, 1805.
2. Riedel, R.; Mera, G.; Hauser, R.; Klonczynski, A. *J. Ceram. Soc. Jpn.* **2006,** *114*, 425.
3. Colombo, P.; Soraru, G. D.; Riedel, R.; Kleebe, A. Polymer Derived Ceramics: Theory and Applications, 1st ed.; DES-tech Publications (United States), **2009.**
4. Ionescu, E.; Kleebe, H.-J.; Riedel, R. *Chem. Soc. Rev., in press.* DOI: 10.1039/C2CS15319J.
5. Li, J.; Salles, V.; Bernard, S.; Gervais, C.; Miele, P. *Chem. Mater.* **2010,** *22*, 2010.
6. Bill, J.; Aldinger, F. *Adv. Mater.* **1995,** *7*, 775.
7. Toutois, P.; Miele, P.; Jacques, S.; Cornu, D.; Bernard, S. *J. Am. Ceram. Soc.* **2006,** *89*, 42.
8. Miele, P.; Bernard, S.; Cornu, D.; Toury, B. *Soft Matter* **2006,** *4*, 249.
9. Salles, V.; Bernard, S.; Brioude, A.; Cornu, D.; Miele, P. *Nanoscale* **2010,** *2*, 215.
10. Schlienger, S.; Alauzun, J.; Michaux, F.; Vidal, L.; Parmentier, J.; Gervais, C.; Babonneau, F.; Bernard, S.; Miele, P.; Parra, J. B. *Chem. Mater.* **2012,** *24*, 88.
11. Alauzun, J. G.; Ungureanu, S.; Brun, N.; Bernard, S.; Miele, P.; Backov, R.; Sanchez, C. *J. Mater. Chem.* **2011,** *21*, 14025.
12. Duperrier, S.; Calin, A.; Bernard, S.; Balan, C.; Miele, P. *Soft Matter* **2006,** *2*, 123.
13. Duperrier, S.; Gervais, C.; Bernard, S.; Cornu, D.; Babonneau, F.; Balan, C.; Miele, P. *Macromolecules* **2007,** *40*, 1018.
14. Duperrier, S.; Bernard, S.; Calin, A.; Sigala, C.; Chiriac, R.; Miele, P.; Balan, C. *Macromolecules* **2007,** *40*, 1028.
15. Münstedt, H. *Soft Matter* **2011,** *7*, 2273.
16. Riedel, R.; Kienzle, A.; Dressler, W.; Ruwisch, L.; Bill, J.; Aldinger, F. *Nature* **1996,** *382*, 796.

17. Weinmann, M.; Schuhmacher, J.; Kummer, H.; Prinz, S.; Peng, J.; Seifert, H. J.; Christ, M.; Müller, K.; Bill, J.; Aldinger, F. *Chem. Mater.* **2000,** *12*, 623.
18. Majoulet, O.; Alauzun, J. G.; Gottardo, L.; Gervais, C.; Schuster, M. E.; Bernard, S.; Miele, P. *Micro. Meso. Mater.* **2011,** *140*, 40.
19. Bernard, S.; Weinmann, M.; Cornu, D.; Miele, P.; Aldinger, F. *J. Eur. Ceram. Soc.* **2005,** *25*, 251.
20. Bernard, S.; Weinmann, M.; Gerstel, P.; Miele, P.; Aldinger, F. *J. Mater. Chem.* **2005,** *5*, 289.
21. Yan, X. B.; Dibandjo, P.; Bernard, S.; Gottardo, L.; Mouttaabidd, H.; Miele, P. *Chem. Mater.* **2008,** *20*, 6325.
22. Bernard, S.; Duperrier, S.; Cornu, D.; Miele, P.; Weinmann, M.; Balan, C.; Aldinger, F. *J. Optoelectron. Adv. Mater.* **2006,** *8*, 648.
23. Gottardo, L.; Bernard, S.; Gervais, C.; Inzenhofer, K.; Motz, G.; Weinmann, M.; Balan, C.; Miele, P. *J. Mater. Chem.* **2012,** *22*, 7739.
24. Jones, R.; Myers, J. K. *J. Organometal. Chem.* **1972, 34, C9.**
25. Weinmann, M.; Kamphowe, T. W.; Fischer, P.; Aldinger, F. *J. Organomet. Chem.* **1999,** *592*, 115.
26. Schuhmacher, J. PhD Thesis, University of Stuttgart, Stuttgart, **2000.**
27. Duperrier, S.; Chiriac, R.; Sigala, C.; Gervais, C.; Bernard, S.; Cornu, D.; Miele, P. *J. Eur. Ceram. Soc.* **2009,** *29*, 851.
28. Hoffmann, M. PhD Thesis, Shaker Verlag, Aaachen, **2001.**
29. Cox, W. P.; Merz, E. H. *J. Polym. Sci.* **1958,** *28*, 619.
30. Han, C. D. (1982) by Cogswell, F. N., Polymer Melt-Rheology - A Guide for Industrial Practice; Wiley, New York, 1981, pp 178.
31. Leonov, A. I.; Prokunin, A. N. Nonlinear Phenomena in Flows of Viscoelastic Polymer Fluids; Chapman & Hall: London, **1994.**
32. Doufas, A. K.; McHugh, A. J.; Miller, C. J. *Non-Newtonian Fluid Mech.* **2000,** *92*, 27.
33. Götz, T.; Klar, A. Unterreiter in Progress in Industrial Mathematics at ECMI 2006; Springer: Berlin, **2008;** p 697.
34. Van Meerveld, J.; Huter, M.; Peters, G. W. M. *J. Non-Newtonian Fluid Mech.* **2008,** *150*, 177.
35. Vogel, R.; Brunig, H.; Beyreuther, R.; Tandler, B.; Voigt, D. *Int. Polym. Process.* **1999,** *14*, 69.
36. Ouyang, T. PhD Thesis, Polytehnica University, Bucharest, **2010.**
37. Beyreuther, R.; Bruning, H. Modelling of Steady State Fibre Formation Process in Melt Spinning in Dynamics of Fibre Formation and Processing Modelling and Application in Fibre and Textile Industry, Springer (Berlin Heidelberg), 2007; p 43.